

Can Metal Cations Electrocatalyze Sulfur Redox Reaction and Suppress Polysulfide Shuttle?

Subramani Kumar,^[a, b] Gitanjali Swain,^[a, b] and Kothandam Krishnamoorthy*^[a, b]

In lithium-sulfur (Li–S) batteries, sulfur undergoes various changes. It switches between cyclic structure and linear structure. The charge on the sulfur varies between a neutral state and a negative charge-bearing state. Due to these changes, the sulfur/polysulfide dissolves in the battery electrolyte. Furthermore, the kinetics of the sulfur redox reaction is sluggish. Therefore, a material that can suppress sulfur/polysulfide dissolution and electrocatalyze sulfur redox reaction is needed. We hypothesize that the polysulfide dissolution can be suppressed if the host exhibits polyvalent electrostatic attraction. Polysulfide is a negative charge-bearing molecule; hence the host must comprise multiple positive charges. Nickel cations with other heteroatoms have been explored as a host in Li–S batteries. The heteroatoms impart additional interactions. The

easier way to circumvent the effect of heteroatoms is the addition of metal salts. However, metal salts can either exhibit monovalent or divalent attraction with polysulfides. Those interactions are weak and we must have polyvalent interaction. Towards this objective, we have designed and synthesized a material that comprises multiple divalent cations that is also devoid of heteroatoms. The Li–S batteries fabricated using the metal cation immobilized graphene showed a maximum specific capacity of 1022 mAh/g at 0.1 C rate. Among the metal cations, nickel cations showed better performance than cobalt cations. Thus, we demonstrate that metal cations immobilized on Graphene can efficiently electrocatalyze the sluggish sulfur redox reaction and suppress the polysulfide dissolution.

Introduction

The sulfur undergoes various structural changes during the charging and discharging of lithium-sulfur (Li–S) batteries. In fact, it switches between cyclic sulfur and linear polysulfide. The charge also varies between neutral and negative charge-bearing states. During this process, the sulfur, as well as polysulfide, dissolve in the battery electrolyte. This leads to the deterioration of battery performance upon charge-discharge cycling of the Li–S battery.^[1] Various approaches have been developed to confine the sulfur into a porous architecture, which in turn was expected to suppress the polysulfides dissolution.^[2,3] Some of these porous materials were able to retain large quantities of polysulfides in the pores, which improved the charge-discharge stability. However, it must be noted that the interaction between the pore walls and sulfur/polysulfide is weak. Therefore, leaching is not controlled to a great extent.^[3,4] Various other non-porous materials have been synthesized to attract sulfur and polysulfide. They include metal carbides, metal nanoparticles, and carbon materials.^[5] Several hosts that have Lewis acid-Lewis base interaction, glucose-sulfur interaction, electrostatic attraction, and chalcogen-sulfur

interaction have been designed and synthesized.^[6–8] Among the non-covalent interactions, polyvalent electrostatic attraction is stronger than most other interactions, hence they have been explored in Li–S batteries. For example, a Nickel based metal-organic framework has been used as a host in Li–S batteries.^[9,10] We used Nickel phthalocyanine exfoliated Graphene as a host.^[11] In these cases, heteroatoms are also present in addition to the cation. The heteroatoms can impart Lewis acid-Lewis base interaction.^[8,9,12]

To understand the impact of electrostatic interaction in suppressing sulfur/polysulfide dissolution, we need to have materials that are devoid of any other type of interaction. At least, the other interaction must be very weak. Polyvalent electrostatic attraction is much stronger than monovalent and divalent electrostatic interaction. Therefore, we cannot use metal salts alone as a host. The metal cations must be part of a host that leads to polyvalent electrostatic attraction with negative charge-bearing polysulfide. Towards this objective, we have chosen Graphene as a host because, we found that Graphene without heteroatoms is not an effective host.^[11] Therefore, we have chosen to decorate the graphene surface with metal cations. The next question is how do we immobilize metal cations on Graphene? We envisioned that the cation- π interaction will facilitate the immobilization of metal cations on the surface of Graphene.^[13,14] Nickel salts were ball milled with the Graphite, which led to the formation of few-layer Graphene with Nickel cations adhering to the surface. Thus, the resultant material comprises positive charges for polyvalent interaction with polysulfides. In our previous work, Nickel cations with heteroatoms have been shown to perform well as hosts in Li–S batteries. Is Nickel unique or does any cation work? To address this question, Graphite was ball-milled with Cobalt salt.^[15] The

[a] Dr. S. Kumar, G. Swain, Dr. K. Krishnamoorthy
Polymer Science and Engineering Division, CSIR-National Chemical Laboratory, Pashan Road, 411008 Pune (India)

E-mail: k.krishnamoorthy@ncl.res.in
Homepage: <http://academic.ncl.res.in/k.krishnamoorthy>

[b] Dr. S. Kumar, G. Swain, Dr. K. Krishnamoorthy
Academy of Scientific and Innovative Research, Kamla Nehru Nagar, 201002 Ghaziabad (India)

 Supporting information for this article is available on the WWW under <https://doi.org/10.1002/batt.202300136>

Cobalt cations decorated Graphene has been used as a host in Li–S batteries.^[6,8,16] Herein, we present the results that corroborate that the Nickel decorated Graphene are an efficient electrocatalyst for sulfur redox reaction. Please note that the metal cation that does not comprise any ligand acts as an efficient electrocatalyst and suppresses the polysulfide dissolution.

Results and Discussion

Graphite was ball-milled with NiSO_4 salt. We envisioned that the Nickel cations will intercalate into the layers of Graphite. The intercalated cations are expected to adhere on the surface of the Graphene due to cation- π interaction.^[13] Furthermore, the cations are expected to repel each other leading to the exfoliation of Graphene from Graphite. After the ball-milling, the samples were washed with a copious amount of dimethylsulfoxide and dried. This sample will be mentioned as G–Ni in the forthcoming discussions. Graphite was also ball-milled with CoCl_2 . This sample will be mentioned as G–Co. The dried samples were studied by Raman spectroscopy. For G–Ni and G–Co, G and 2D bands appeared at 1570 cm^{-1} and 2653 cm^{-1} , respectively. The D and D' bands appeared at 1330 cm^{-1} and 1610 cm^{-1} , respectively (Figure 1a). The ratio of intensities of D and G bands ($I_{\text{D}}/I_{\text{G}}$) provides information about the Graphene layers.^[14] The $I_{\text{D}}/I_{\text{G}}$ for G–Ni and G–Co are 0.45 and 0.35, respectively. On the other hand, $I_{\text{D}}/I_{\text{G}}$ is 0.08 for Graphite. The high $I_{\text{D}}/I_{\text{G}}$ observed in case of G–Ni and G–Co indicates the presence of few-layer Graphene in these two samples. The $I_{\text{D}}/I_{\text{D}'}$ provides information about the defects in the Graphene.^[14,17] The $I_{\text{D}}/I_{\text{D}'}$ were found to be 1.05 for G–Ni and G–Co. $I_{\text{D}}/I_{\text{D}'}$ less than 3.5 indicates the absence of sp^3 and basal plane defects. This indicates that the Graphene exfoliated using metal salts are

of high quality. The samples were subjected to XRD analysis. The d spacing was found to be 3.31 \AA (Figure S1a), which increased to 3.34 \AA for G–Co (Figure S1b). The d-spacing further increased to 3.37 \AA for G–Ni (Figure S1c). TEM imaging was used to identify the number of Graphene layers present in Graphite, G–Ni, and G–Co. In Graphite, eighty Graphene layers were found (Figure S2a). In the case of G–Co, eight Graphene layers were found (Figure 1b). The EDAX images indicate that the cobalt cations exist as clusters in various places (Figure S2b). In the case of G–Ni, five layers of Graphene were found (Figure 1c). The EDAX images indicate that the Nickel cations are present as large clusters. In fact, the clusters are significantly larger than the cobalt clusters of G–Co (Figure S2c). The X-Ray photoelectron spectroscopy (XPS) spectrum for G–Ni comprises the $\text{Ni } 2\text{p}_{3/2}$ and $\text{Ni } 2\text{p}_{1/2}$ spin orbits at 857.4 eV and 875.2 eV , respectively. The XPS spectrum of C 1s shows the existence of sp^2C (284.2 eV), sp^3C (285.3 eV), C=O (285.8 eV) and C=O (288.9 eV). Also, the S 2p spectrum consists of $\text{S } 2\text{p}_{3/2}$ (162.6 eV) and $\text{S } 2\text{p}_{1/2}$ (169.6 eV) and the O 1s spectrum consists of SO_4^{2-} (532.2 eV) and O–H (533.4 eV) as shown in Figure S3. The O–H is likely due to the moisture present in NiSO_4 . For the G–Co, the XPS spectrum comprises $\text{Co } 2\text{p}_{3/2}$ (781.7 eV) and $\text{Co } 2\text{p}_{1/2}$ (797.6 eV). The C 1s spectrum demonstrates the sp^2C (284.4 eV), sp^3C (285.2 eV), C=O (285.7 eV) and C=O (289.2 eV) and the Cl 2p spectrum exists the $\text{Cl } 2\text{p}_{3/2}$ (199.1 eV) and $\text{Cl } 2\text{p}_{1/2}$ (200.7 eV) are shown in Figure S4. The quantity of metal cation ($\text{Co}^{2+}/\text{Ni}^{2+}$) present in the materials were determined through inductively coupled plasma-optical emission spectroscopy analysis, found that 23.7% and 18.5% of Cobalt and Nickel ion for G–Co, G–Ni, respectively (Table S1).

With this information in hand, we proceeded to study the efficacy of sulfur loading on G–Co and G–Ni. The TGA experiment indicates the sulfur loading is 69.1% in the case of G–Ni and 62.8% for G–Co (Figure S5). In order to study how efficiently the G–Co and G–Ni absorb polysulfides, a 5 ml solution of S_6^{2-} was added to 1 mg of G–Co and G–Ni. The UV-vis absorption spectra of S_6^{2-} solution exhibited two peaks at 263 nm and 280 nm (Figure 1d). As an internal standard, Diketopyrrolopyrrole-12 (DPP-12) (Figure S6) was added. This molecule exhibits absorption maxima at 509 nm and 547 nm . The UV-vis absorption spectra of the aliquots taken from all the vials showed the same absorbance. However, the aliquots taken after 24 hrs exhibited significantly different absorbance. The absorbance decreased in the following order $\text{S}_6^{2-} > (\text{S}_6^{2-} + \text{Graphite}) > (\text{S}_6^{2-} + \text{G–Co}) > (\text{S}_6^{2-} + \text{G–Ni})$. Thus, the Nickel cations show better adsorption of polysulfide compared to Cobalt cations. Please note that the absorbance of DPP remained constant, indicating the variation in the absorbance of S_6^{2-} is due to the absorption of the polysulfide on Graphite and exfoliated Graphene such as G–Co and G–Ni. One of the objectives of this work is to study the electrocatalytic activity of metal cations. To study this aspect, symmetric cells were fabricated using either G–Ni as electrodes or G–Co as electrodes. This method has been well-established in the literature to study the electrocatalysis of sulfur.^[18] The cyclic voltammogram of the cells was recorded between -1 V and $+1\text{ V}$ (Figure 2a). The first oxidation peak at 0.09 V for G–Ni and at 0.35 V for

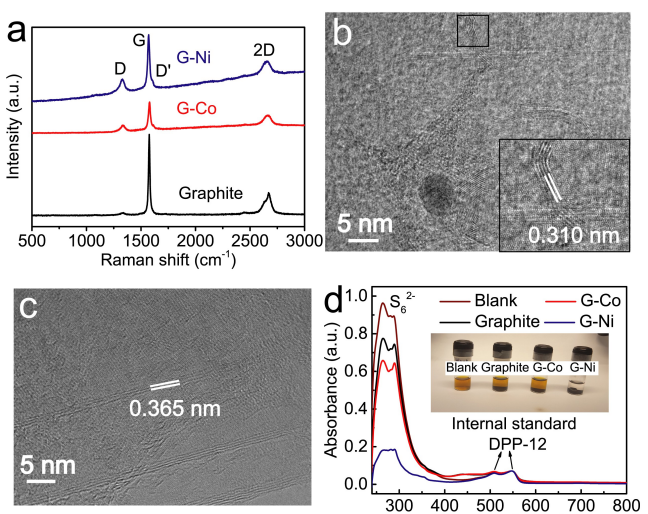


Figure 1. a) Raman spectra showing D, D', G and 2D bands of Graphite, G–Co and G–Ni. HRTEM imaging of b) G–Co and c) G–Ni. d) UV-Vis spectra of Li_2S_6 solution with Graphite, G–Co and G–Ni. The insert shows the de-coloration of the solution due to attraction between Li_2S_6 and G–Ni.

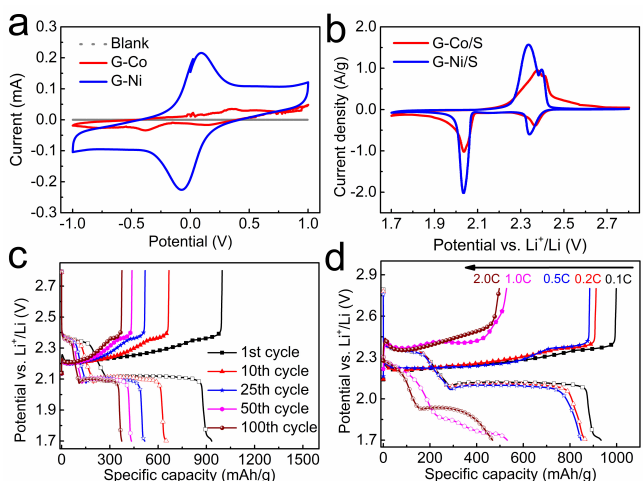


Figure 2. Cyclic voltammogram of a) symmetric cell using G-Co and G-Ni comprised electrodes with scan rate of 6 mV/s and b) Li-S cells with scan rate of 0.1 mV/s using G-Co/S and G-Ni/S. Charge/discharge profile of c) Li-S cell with G-Co/S at 0.1 C rate and d) first cycle at various rates (0.1 C, 0.2 C, 0.5 C, 1 C and 2 C).

G-Co correspond to the conversion of Li_2S to Li_2S_6 . The second extremely weak oxidation peak at 0.53 V for G-Ni and at 0.56 V for G-Co correspond to the conversion of Li_2S_6 to S_8 . In the reverse scan, the first reduction peaks at -0.07 V (G-Ni) and -0.38 V (G-Co) are due to reduction of S_8 to Li_2S_6 . The second reduction peak at -0.55 V (G-Ni) and -0.76 V (G-Co) are due to reduction of Li_2S_6 to Li_2S .

In the next set of experiments, Li-S batteries were fabricated using the exfoliated Graphene, Sulfur, conducting carbon, and binder. The CV of the batteries was recorded at a scan rate of 0.1 mV/s. In the forward scan of the battery comprising G-Co, two peaks were observed at 2.38 V and 2.41 V (Figure 2b). These two peaks correspond to $\text{Li}_2\text{S}/\text{Li}_2\text{S}_2 \rightarrow \text{Li}_2\text{S}_n$ ($n=4$ to 8) and Li_2S_n ($n=4$ to 8) $\rightarrow \text{Li}_2\text{S}/\text{S}_8$. In the reverse scan, two peaks were observed at 2.04 V and 2.37 V (Figure 2b). Similarly, two peaks were observed at 2.4 V and 2.33 V during the forward scan and two peaks were also observed at 2.04 V and 2.34 V in the reverse scan while using G-Ni as electrode material (Figure 2b). Usually, in the forward scan, one peak is observed due to poor electrocatalytic activity of the host material. In fact, we did observe only a single peak while using doped Graphene as electrode.^[11] The two well-defined peaks in the forward scan while using G-Co and G-Ni as electrodes is an indication of efficient electrocatalysis of Sulfur redox reaction. The Li-S battery prepared using G-Co was subjected to charge-discharge experiment. At 0.1 C, the specific capacity at the first cycle was 998 mAh/g. This is significantly higher than Graphene without metal ions. Upon charge-discharge cycling, the specific capacity decreased to 375 mAh/g at the 100th cycle (Figure 2c). The retention of specific capacity is 38%. Upon increasing the C rate, the specific capacity at the first cycle also decreased. The decrease in the specific capacity at the first cycle decreased in the following order, 0.1 C (998 mAh/g) $>$ 0.2 C (912 mAh/g) $>$ 0.5 C (885 mAh/g) $>$ 1 C (528 mAh/g) $>$ 2 C (494 mAh/g) (Figure 2d).

At the 100th charge-discharge cycle, the specific capacity retention is as follows, 0.1 C (38%) $>$ 0.2 C (37%) $<$ 0.5 C (46%) $<$ 1 C (72%) $<$ 2 C (74%). From this data, it is clear that the fading is significantly lower upon increase in C rate. However, we must also keep in mind that the initial specific capacity is low at higher C rates. The rate performance of the Li-S battery was studied by changing the C rate of charge-discharge of a battery. At 0.1 C rate, the specific capacity was 940 mAh/g, which decreased upon increase in C rate. At 2 C rate, the specific capacity was 356 mAh/g. Subsequently, the battery's performance was studied at 0.1 C. The specific capacity increased to 714 mAh/g, which is \sim 230 mAh/g lower than the specific capacity observed at 0.1 C measured at the start of the experiment (Figure 3a). The degradation of battery performance is due to the dissolution of sulfur/polysulfide. The batteries were subjected to 500 charge-discharge cycling. The specific capacity retention of the batteries as a function of C rates are 19% (0.2 C) 26% (0.5 C) 48% (1 C) 45% (2 C) (Figure 3b). The specific capacity retention is not impressive.

In the next set of experiments, Li-S batteries were fabricated using G-Ni as the host material. At 0.1 C, the specific capacity was 1022 mAh/g, which is higher than that was observed for batteries prepared using G-Co as the host material. At 100th cycle, the specific capacity decreased to 926 mAh/g (Figure 3c). The specific capacity retention is 91%, which is impressive. Furthermore, we measured the specific capacity of the battery at various C rates. The specific capacity at the first cycle as a function of various C rates varied as follows, 0.1 C (1022 mAh/g) $>$ 0.2 C (996 mAh/g) $>$ 0.5 C (960 mAh/g) $>$ 1 C (797 mAh/g) $>$ 2 C (738 mAh/g). At 100th cycle, the specific capacity retention as a function of C rates is 0.1 C (91%) $>$ 0.2 C (78%) $>$ 0.5 C (68%) $<$ 1 C (75%) $>$ 2 C (73%) (Figure 3d). From this data, it is clear that the specific capacity retention is comparable as a function of C rate variation except at 0.1 C. We proceeded to study the rate performance characteristics of the battery. The specific capacity

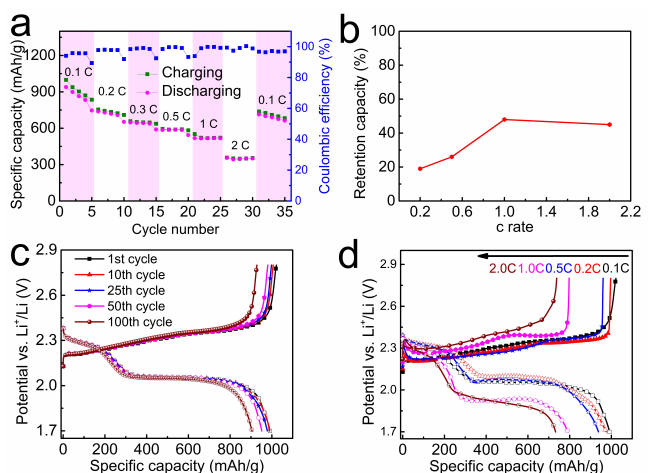


Figure 3. a) Rate performance studies, b) percentage retention with respect to various C rates of Li-S cell using G-Co. Charge/discharge profile of c) Li-S cell using G-Ni at 0.1 C rate for 100 cycles and d) first cycle of different rates (0.1 C, 0.2 C, 0.5 C, 1 C and 2 C).

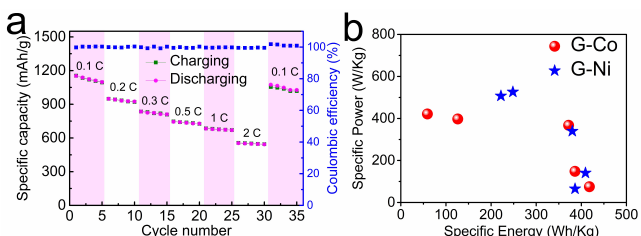


Figure 4. a) Rate performance studies of Li/S cell using G-Ni/S and b) Ragone plot for Li-S cell using G-Co and G-Ni comprised sulfur electrodes.

at 0.1 C was 1153 mAh/g, which decreased to 554 mAh/g while the battery was subjected to charge-discharge at 2 C rate. Subsequently, the battery's specific capacity was measured at 0.1 C. The specific capacity was found to be 991 mAh/g, which is comparable to the specific capacity measured at 0.1 C at the start of the experiment (Figure 4a). From this experiment, we conclude that the sulfur/polysulfide dissolution is insignificant while using G-Ni as a host material. Considering the battery's impressive performance, we studied the battery's stability as a function of 500 charge-discharge cycling. The specific capacity retention was 57% at 0.1 C. The specific retention was 49% and 38% for 0.2 C and 2 C, respectively (Figure S7). Thus, the specific capacity retention, as well as the specific capacity of the batteries fabricated using G-Ni is better than G-Co. The other question is, does the adherence of metal cations on Graphene improve battery performance? For example, if the nickel salt is blended with graphite (situation prior to ball milling of graphite with nickel salts), will the battery perform as good as G-Ni? To test this, Graphite was mixed with NiSO_4 and this sample will be mentioned as Graphite-Ni. Li-S batteries were fabricated using Graphite-Ni. All other experimental parameters are similar to the Li-S battery fabricated using G-Ni. The specific capacity of the battery was measured at two C rates. At 0.5 C, the discharge capacity of the first cycle was 470 mAh/g (Figure S16), which is half of that observed for batteries fabricated using G-Ni. At 100 cycles, the specific capacity decreased to 234 mAh/g, which is about three times lower than that was observed for G-Ni based batteries. At 1 C rate, the specific capacity of the first cycle for Graphite-Ni batteries was 382 mAh/g (Figure S17), which is half that of the batteries with G-Ni batteries. A similar trend was observed at 100 cycles. Thus, it is essential to ball-mill Graphite with metal salts and obtain metal cation adhered Graphene to facilitate polyvalent interaction and electrocatalysis. The Ragone plot was computed with the specific energy and specific power (Figure 4b). The G-Ni based batteries exhibited maximum specific energy of 409 Wh/kg and a maximum specific power of 526 W/kg.

Conclusions

In conclusion, we prepared cation-decorated graphene by ball milling NiSO_4 and CoCl_2 . The Nickel decorated graphene (G-Ni) was found to attract polysulfide effectively, indicating its ability

as a good host in Li-S battery. The cyclic voltammogram corroborated the electrocatalytic activity of G-Ni. The batteries fabricated using G-Ni exhibited a maximum specific capacity of 1022 mAh/g at 0.1 C rate. The battery retained 91% of its initial specific capacity upon 100 charge-discharge cycles and 57% at the 500th cycle. The data clearly proved that the Nickel cations are capable of electrocatalysing the sluggish Sulfur redox reaction and suppressing the polysulfide dissolution in the battery electrolyte.

Experimental Section

Chemicals and materials

The following chemicals were used as procured. Graphite powder (Sigma-Aldrich, <20 μm), $\text{NiSO}_4 \cdot 6\text{H}_2\text{O}$ (Sigma-Aldrich), $\text{CoCl}_2 \cdot 6\text{H}_2\text{O}$ (Sigma-Aldrich), dimethylformamide (DMF, Merck, AR grade), N-Methyl-2-pyrrolidone (NMP, Merck, AR grade), Super P carbon (Imerys Graphite & Carbon Switzerland Ltd., Switzerland), Poly(vinylidene fluoride) (PVDF, Kynar HSV900, Arkema Inc., USA), Li metal (Global nanotech), Celgard 2325 (Porepore, USA), bis(trifluoromethane)sulfonimide lithium salt (LiTFSI , Sigma-Aldrich, 99.95%), lithium nitrate (LiNO_3 , Sigma-Aldrich, 99.99%), 1,3-dioxolane (DOL, Sigma Aldrich, 99.8%), and 1,2-dimethoxyethane (DME, Sigma-Aldrich, 99.5%).

Preparation of G-Co and G-Ni

The graphite powder was exfoliated using Ni^{2+} or Co^{2+} salts as an intercalator. The graphite (0.5 g) and NiSO_4 or CoCl_2 (2.5 g), were treated for mechanical ball-milling process in an Agate ball mill grinder (250 mL) and six balls with diameter of 1 cm have been used. The milling was carried out at 200 rpm for 60 min. The as-exfoliated materials were washed with copious amount of DMF and dried at 120 °C under vacuum for 24 h.

Preparation of G-Co/S and G-Ni/S

The sulfur encapsulation was carried out using melt-diffusion method. The cation doped graphene layers were dried well before the process. The elemental sulfur and cation doped graphene (G/Co or G-Ni) (80:20 ratio) were grinded well and transferred into alumina crucible and heated at 155 °C under argon atmosphere for 16 h.

Materials characterizations

The TEM and HRTEM images were recorded with Tecnai G2 20 STWIN transmission electron microscope and Jeol 1200 EX transmission electron microscope, respectively. The carbon-coated copper grids (200) were obtained from Ted Pella. The samples for TEM imaging were prepared by dispersing 1 mg of material in DMF and drop casted onto carbon-coated copper grid and dried at 80 °C for 24 h. The Raman spectroscopy measurements were performed with LabRam spectrometer (HJY, France) equipped with a laser wavelength of 632 nm. The X-ray diffraction spectra were recorded with PANalytical instrument was operated using $\text{Cu K}\alpha$ radiation ($\lambda = 1.542 \text{ \AA}$) at a scanning rate of 2° min^{-1} and a step size of 0.02° in 2θ with operating voltage 40 kV and operating current 30 mA to acquire the X-ray diffraction spectra. The X-ray photoelectron spectroscopy measurements were done on Thermo Kalpha+ spectrometer using $\text{Al K}\alpha$ radiation with an energy of 1486.6 eV. All

the spectra were charge corrected with reference to C 1s at 284.6 eV. The peak fittings were carried out using CasaXPS software. And the thermogravimetric analyzes were carried out on SDTQ600 TG-DTA analyzer in a nitrogen environment with a ramp of $5^{\circ}\text{C min}^{-1}$. The ICP-OES analysis was carried out using SPECTRO ARCOS FHS12 analyzer.

Li-S cell fabrication and electrochemical characterizations

The slurry was prepared using sulfur encapsulated cation doped graphene (G-Co/S or G-Ni/S) as an active material, Super P carbon and PVDF with the ratio of 7:2:1 by grinded well and coated onto the carbon coated aluminum foil and dried at 60°C for 16 h. The Li-S cells were fabricated using the above coated disc electrode as working electrode (12 mm dia), Lithium metal as reference as well as counter electrode. 1 M LiTFSI as an electrolyte and 0.2 M LiNO₃ as an additive in 1,3-dioxolane (DOL) and 1,2-dimethoxyethane (DME) (1:1 volume ratio) were used, and Celgard 2325 (Thickness 25 μm) as separator. The mass of loaded active materials was 1 mg/cm² and the volume of electrolyte used in cell is 15 μL . The coin cells (2032 type) were fabricated in an argon filled glovebox (MBRAUN, O₂<0.1 ppm, H₂O<0.1 ppm). The electrochemical chemical testings were carried out with potential window of 1.7–2.8 V at 25°C . The cyclic voltammetry techniques were carried out using multichannel Autolab MAC80038 instrument. The cyclic charge-discharge experiments were carried out in Neware battery testers. The specific energy (Wh/Kg) of the cells were carried out by calculating the area under the discharge curves and specific power (W/kg) by specific energy/time (h).

Polysulfide adsorption and symmetric cell tests

A 0.2 M of Lithium polysulfide (Li₂S₆) solution was prepared by solvating the elemental sulfur and Lithium sulfide (Li₂S) with the molar ratio of 5:1, in the mixture of DOL and DME (1:1 volume ratio) solvents. The solution was vigorously stirred at 50°C for 24 h. For polysulfide adsorption test, 5 mg of the cation doped graphene (G-Co or G-Ni) was transferred into the separate vials contain 2 mL of Lithium polysulfide solution. The symmetric cells were fabricated using the identical electrodes comprised of G-Co or G-Ni. The 0.2 M Li₂S₆ catholyte has been used and cyclic voltammograms of the cells were demonstrated at 6 mV/s with the potential window of –1.0 V to +1.0 V. The polysulfide adsorption tests and symmetric cell fabrications were carried out inside argon filled glovebox.

Sample preparation for ICP-OES analysis

The cation doped graphene (G-Co or G-Ni) (15 mg) were taken separately and added to 5 mL of freshly prepared aqua regia. The samples were digested by thermal treatment and concentrated up to 2 mL. Further, diluted by adding 15 mL of de-ionized water and filtered through syringe (0.22 micron). The analyses were carried out under argon atmosphere.

Acknowledgements

S. K. thanks the Department of Science and Technology for the Fellowship, G. S. thanks CSIR for the Fellowship. K. K. thanks Aeronautics Research and Development Board - India for funding (ARDB/01/2032010/M/I).

Conflict of Interests

The authors declare no conflict of interest.

Data Availability Statement

The data that support the findings of this study are available from the corresponding author upon reasonable request.

Keywords: lithium-sulfur batteries · metal cations · graphene · electrocatalysis · polysulfides

- [1] a) A. Manthiram, Y. Fu, Y.-S. Su, *Acc. Chem. Res.* **2013**, *46*, 1125–1134; b) A. Rosenman, E. Markevich, G. Salitra, D. Aurbach, A. Garsuch, F. F. Chesneau, *Adv. Energy Mater.* **2015**, *5*, 1500212; c) X. Ji, L. F. Nazar, *J. Mater. Chem.* **2010**, *20*, 9821–9826; d) A. Manthiram, Y. Fu, S.-H. Chung, C. Zu, Y.-S. Su, *Chem. Rev.* **2014**, *114*, 11751–11787.
- [2] a) A. Manthiram, S.-H. Chung, C. Zu, *Adv. Mater.* **2015**, *27*, 1980–2006; b) X. Fan, W. Sun, F. Meng, A. Xing, J. Liu, *Green Energy & Environ.* **2018**, *3*, 2–19; c) L. Yang, Q. Li, Y. Wang, Y. Chen, X. Guo, Z. Wu, G. Chen, B. Zhong, W. Xiang, Y. Zhong, *Ionics* **2020**, *26*, 5299–5318.
- [3] A. Eftekhar, D.-W. Kim, *J. Mater. Chem. A* **2017**, *5*, 17734–17776.
- [4] a) W. Kang, N. Deng, J. Ju, Q. Li, D. Wu, X. Ma, L. Li, M. Naebe, B. Cheng, *Nanoscale* **2016**, *8*, 16541–16588; b) K. Han, J. Shen, S. Hao, H. Ye, C. Wolverton, M. C. Kung, H. H. Kung, *ChemSusChem* **2014**, *7*, 2545–2553; c) M.-Q. Zhao, X.-F. Liu, Q. Zhang, G.-L. Tian, J.-Q. Huang, W. Zhu, F. Wei, *ACS Nano* **2012**, *6*, 10759–10769.
- [5] a) C. Zhang, L. Cui, S. Abdolhosseinzadeh, J. Heier, *InfoMat.* **2020**, *2*, 613–638; b) X.-J. Hong, C.-L. Song, Z.-M. Wu, Z.-H. Li, Y.-P. Cai, C.-X. Wang, H. Wang, *Chem. Eng. J.* **2021**, *404*, 126566; c) H.-J. Peng, G. Zhang, X. Chen, Z.-W. Zhang, W.-T. Xu, J.-Q. Huang, Q. Zhang, *Angew. Chem. Int. Ed.* **2016**, *55*, 12990–12995; d) S.-F. Ng, M. Y. L. Lau, W.-J. Ong, *Adv. Mater.* **2021**, *33*, 2008654; e) K.-X. Huang, J. Hua, G.-G. Chang, Z. Li, G. Tian, M.-J. Chen, J.-X. Li, S.-C. Ke, X.-Y. Yang, B. Chen, *Small* **2021**, *17*, 2002811; f) Y. Tsao, H. Gong, S. Chen, G. Chen, Y. Liu, T. Z. Gao, Y. Cui, Z. Bao, *Adv. Energy Mater.* **2021**, *11*, 2101449; g) M. Shaibani, S. Mirshekarloo Meysam, R. Singh, D. Easton Christopher, M. C. D. Cooray, N. Eshraghi, T. Abendroth, S. Dörfler, H. Althues, S. Kaskel, F. Hollenkamp Anthony, R. Hill Matthew, M. Majumder, *Sci. Adv.* **2020**, *6*, eaay2757; h) Z. Lian, M. Yang, F. Jan, B. Li, *J. Phys. Chem. Lett.* **2021**, *12*, 7053–7059; i) Y. Zhong, K. R. Yang, W. Liu, P. He, V. Batista, H. Wang, *J. Phys. Chem. C* **2017**, *121*, 14222–14227; j) X. Han, Z. Zhang, X. Xu, *J. Mater. Chem. A* **2021**, *9*, 12225–12235.
- [6] Y. Li, S. Lin, D. Wang, T. Gao, J. Song, P. Zhou, Z. Xu, Z. Yang, N. Xiao, S. Guo, *Adv. Mater.* **2020**, *32*, 1906722.
- [7] a) S. Niu, W. Lv, C. Zhang, F. Li, L. Tang, Y. He, B. Li, Q.-H. Yang, F. Kang, *J. Mater. Chem. A* **2015**, *3*, 20218–20224; b) Q. Wu, Y. Chen, X. Hao, T. Zhu, Y. Cao, W. Wang, *J. Electrochem. Soc.* **2021**, *168*, 120516; c) H. Ye, J. Y. Lee, *Small Methods* **2020**, *4*, 1900864; d) Y. Huang, M. Shaibani, T. D. Gamot, M. Wang, P. Jovanović, M. C. Dilusha Cooray, M. S. Mirshekarloo, R. J. Mulder, N. V. Medhekar, M. R. Hill, M. Majumder, *Nat. Commun.* **2021**, *12*, 5375; e) Q. Jin, Y. Yan, C. Hu, Y. Zhang, X. Wang, C. Liang, *Nanomaterials* **2022**, *12*, 886.
- [8] Z. Du, X. Chen, W. Hu, C. Chuang, S. Xie, A. Hu, W. Yan, X. Kong, X. Wu, H. Ji, L.-J. Wan, *J. Am. Chem. Soc.* **2019**, *141*, 3977–3985.
- [9] J. Zheng, J. Tian, D. Wu, M. Gu, W. Xu, C. Wang, F. Gao, M. H. Engelhard, J.-G. Zhang, J. Liu, J. Xiao, *Nano Lett.* **2014**, *14*, 2345–2352.
- [10] S. Wang, F. Huang, Z. Zhang, W. Cai, Y. Jie, S. Wang, P. Yan, S. Jiao, R. Cao, *J. Energy Chem.* **2021**, *63*, 336–343.
- [11] S. Kumar, K. Krishnamoorthy, *Batteries & Supercaps* **2021**, *5*, e202100229.
- [12] a) M. A. Hossain, S. Tulaphol, A. K. Thapa, M. S. Rahaman, J. B. Jasinski, H. Wang, M. K. Sunkara, J. Syzdek, O. K. Ozdemir, J. M. Ornstein, N. Sathitsuksanoh, *ACS Appl. Energ. Mater.* **2021**, *4*, 13450–13460; b) X.-Q. Niu, X.-L. Wang, D. Xie, D.-H. Wang, Y.-D. Zhang, Y. Li, T. Yu, J.-P. Tu, *ACS Appl. Mater. Interfaces* **2015**, *7*, 16715–16722; c) H. Duan, C. Wang, G. Li, H. Tan, W. Hu, L. Cai, W. Liu, N. Li, Q. Ji, Y. Wang, Y. Lu, W. Yan, F. Hu, W. Zhang, Z. Sun, Z. Qi, L. Song, S. Wei, *Angew. Chem. Int. Ed.* **2021**, *60*, 7251–7258; d) J. Kang, Y. Xue, J. Yang, Q. Hu, Q. Zhang, L. Gu, A. Selloni, L.-M. Liu, L. Guo, *J. Am. Chem. Soc.* **2022**, *144*, 8969–8976; e) Y. He, L. Liu,

- C. Zhu, S. Guo, P. Golani, B. Koo, P. Tang, Z. Zhao, M. Xu, C. Zhu, P. Yu, X. Zhou, C. Gao, X. Wang, Z. Shi, L. Zheng, J. Yang, B. Shin, J. Arbiol, H. Duan, Y. Du, M. Heggen, R. E. Dunin-Borkowski, W. Guo, Q. J. Wang, Z. Zhang, Z. Liu, *Nat. Catal.* **2022**, *5*, 212–221; f) J. Kang, X. Qiu, Q. Hu, J. Zhong, X. Gao, R. Huang, C. Wan, L.-M. Liu, X. Duan, L. Guo, *Nat. Catal.* **2021**, *4*, 1050–1058.
- [13] G. Zhao, H. Zhu, *Adv. Mater.* **2020**, *32*, 1905756.
- [14] V. León, A. M. Rodríguez, P. Prieto, M. Prato, E. Vázquez, *ACS Nano* **2014**, *8*, 563–571.
- [15] V. León, M. Quintana, M. A. Herrero, J. L. G. Fierro, A. De La Hoz, M. Prato, E. Vázquez, *Chem. Commun.* **2011**, *47*, 10936–10938.
- [16] Z. Zhang, C. Chen, J. Xu, Z. Lin, Z. Lin, *ACS Appl. Energ. Mater.* **2022**, *5*, 4691–4697.
- [17] A. M. Rodríguez, V. J. González, V. León, M. A. Herrero, A. B. Muñoz-García, M. Pavone, P. Prieto, A. De La Hoz, E. Vázquez, *J. Phys. Mater.* **2020**, *3*, 034011.
- [18] a) R. Wang, C. Luo, T. Wang, G. Zhou, Y. Deng, Y. He, Q. Zhang, F. Kang, W. Lv, Q.-H. Yang, *Adv. Mater.* **2020**, *32*, 2000315; b) Z. Liang, D. Yang, P. Tang, C. Zhang, J. Jacas Biéndicho, Y. Zhang, J. Llorca, X. Wang, J. Li, M. Heggen, J. David, R. E. Dunin-Borkowski, Y. Zhou, J. R. Morante, A. Cabot, J. Arbiol, *Adv. Energy Mater.* **2021**, *11*, 2003507; c) J. He, A. Bhargav, A. Manthiram, *ACS Nano* **2021**, *15*, 8583–8591.

Manuscript received: March 31, 2023

Revised manuscript received: July 18, 2023

Accepted manuscript online: July 24, 2023

Version of record online: August 4, 2023